IECE

IECE Transactions on Internet of Things
http://dx.doi.org/10.62762/TIOT.2024.528361

RESEARCH ARTICLE

Detection of Arctic Sea Ice Using 89 GHz Microwave Radiometer Channels

Yue Zhao[1,*], **Xingdong Wang**[1] **and Changfeng Luo**[1]

[1] College of Information Science and Engineering, Henan University of Technology, Zhengzhou 450001, China

Abstract

Sea ice is a crucial component of the cryosphere, and extensive research has been conducted on sea ice using microwave remote sensing due to its robustness against cloud cover and illumination variations. This paper focuses on classifying Arctic sea ice based on microwave remote sensing data. Leveraging the high stability of microwave radiometers, we analyze the characteristics of different sea ice types across the Arctic region in January 2017 using high-resolution AMSR-E/AMSR2 data at the 89 GHz frequency band. Data at this frequency are less susceptible to cloud and water vapor interference, while lower frequency bands have traditionally been more commonly used in similar studies. However, our study emphasizes the significance of the 89 GHz frequency band, which offers high-resolution data for distinguishing between multi-year ice, first-year ice, and open water. The brightness temperature differences among these sea ice types are analyzed, and a method based on these differences is proposed for classification. The fine tree algorithm in MATLAB's decision tree toolbox is employed to generate the classification results.

Keywords: Sea ice classification, Arctic, Microwave remote sensing, Decision tree.

Academic Editor:
Jinchao Chen

Submitted: 09 February 2024
Accepted: 26 March 2024
Published: 07 April 2024

Vol. 1, **No.** 1, 2024.
10.62762/TIOT.2024.528361

***Corresponding author:**
✉ Yue Zhao
15639785262@163.com

Citation
Zhao, Y., Wang, X., & Luo, C. (2024). Detection of Arctic Sea Ice Using 89 GHz Microwave Radiometer Channels. IECE Transactions on Internet of Things, 1(1), 36–43.

1 Introduction

In recent years, the climate in all parts of the world has changed a lot, except for all kinds of extreme weather events are gradually increasing, more and more people are concerned about the problem of global environmental change. The Arctic region, in particular, has a great impact on global climate change, so many environmental changes are becoming more and more obvious. The mass balance of small Arctic glaciers is affected. The extent of Arctic sea ice has been shrinking in recent decades, while the area covered by snow has been shrinking. In the 20th century, temperatures in the Arctic reached their highest levels in centuries. Because the environment is affected, many regional plants and animals are slowly moving northward. All these clearly show that the changes of Arctic sea ice have a great impact on nature, which makes us living on the earth have to pay attention to these problems.

An important component of the cryosphere is sea ice, which regulates the global climate. The Earth's surface is covered with 25 million square kilometers of sea ice, about 7 percent of the world's seawater. Sea ice plays a very important role in the study of climate and oceans [1]. Sea ice is also a source of cold water in the Antarctic and Arctic Poles and affects the global circulation of climate. Moreover, sea ice plays a very important role in winter. In this season, the atmosphere is much lower than sea water, so sea ice can directly isolate the temperature between them, affecting heat transfer and playing the role of heat insulation. And sea ice can also affect the radiation exchange between the atmosphere and the ocean.

When there is snow on the sea ice, the reflectivity of radiation reaches 80%, and when the sea water is not covered with sea ice and snow, the reflectivity is less than 10%. Therefore, there is a great difference in the reflection of the sea with or without sea ice, and it directly affects the absorption and reflection of the solar radiation by the sea. So if a large area of the ocean is covered with sea ice, it directly reduces the absorption of solar radiation by the ocean, because sea ice itself is very reflective. So the presence or absence of sea ice has a significant impact on the exchange of a lot of energy between the ocean and the atmosphere, which has a huge impact on the global climate and the ecological environment [2, 13–15].

We can often learn from the news that the freezing of sea ice will seriously affect the time and cost of shipping during the passage of ships. It is necessary to break the sea ice so as to prevent ships from passing. Therefore, the formation or drift of sea ice has a serious impact on shipping and polar exploration. In recent years, with the global warming, sea ice is melting on a large scale, because the melting of the Arctic sea ice may open up lanes of the Atlantic and Pacific Oceans, which plays a great role in the maritime transportation. The opening of these shipping lanes affects the economic trade in East Asia [3].

Due to the above impacts of sea ice on the environment and climate, the detection of sea ice is of great significance. The monitoring of sea ice plays a very important role in maritime transportation and various Marine activities, in addition to the impacts on the climate and environment [4]. The exploration of sea ice is of great significance to human survival in many ways.

Figure 1

2 Study Area and Data

2.1 Study area

The Arctic is a region of great concern to human beings. The sea ice studied in this paper is the whole non-land area north of 60 degrees north latitude. The center of the Arctic is the Arctic Ocean, because the Arctic Ocean is surrounded by the Eurasian continent and North America [5].

In a kind of closed area, which is a geographical condition where sea ice is more likely to form. The Arctic is a region that plays a decisive role in global climate change, and it has all kinds of resources that we need, as well as important strategic positions. It is of great value to study the sea ice in the Arctic Ocean for maritime transportation and various operations.

2.2 Data

The AMSR-E(Advanced Microwave Scanning Radiometer for EOS Aqua), launched in 2002 aboard the Aqua satellite, provided data from June 2002 through October 2011. The AMSR-E has a scan bandwidth of 1450km and a total of 12 channels. The differences between them are shown in Table 1.

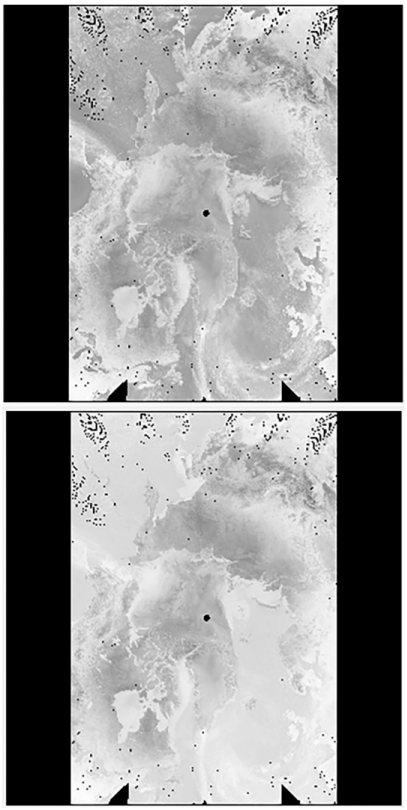

Figure 2. Image of data source.

In this paper, the brightness temperature data of 89 GHz on January 1, 2017 downloaded from the Earth

Table 1. Basic parameters of AMSR-E and AMSR-2 sensors.

Sensors	Satellite platform	Year of operation	Frequency (GHz) and mode of polarization	Spatial resolution (km)
AMSR-E	Aqua	2002-2011	6.93 H/V	73 ×43
			10.65 H/V	51 × 30
			18.7 H/V	27 × 16
			23.8 H/V	31 × 18
			36.5 H/V	14 × 8
			89.0 H/V	6 × 4
AMSR-2	GCOM-W1	2012-now	6.93 H/V	62 × 35
			7.3 H/V	62 × 35
			10.65 H/V	42 × 24
			18.7 H/V	22 × 14
			23.8 H/V	19 × 11
			36.5 H/V	12 × 7
			89.0 H/V	5 × 3

Data Search system of NASA is used. Remote sensing satellite AMSR-2(Advanced Microwave Scanning Radiometer for EOS) calculated the distribution of multi-year ice from the brightness temperatures of vertical and horizontal polarization in the 89GH z band for sea ice classification. The biggest advantage of AMSR-2 is its higher resolution. Especially in the 89GHz band, the resolution of AMSR-E can reach 4 km × 6 km. Therefore, the experiment in this chapter only classifies the sea ice in January 2017, with a time resolution of one day. Fig. 2. shows the original image of the data used in this experiment.

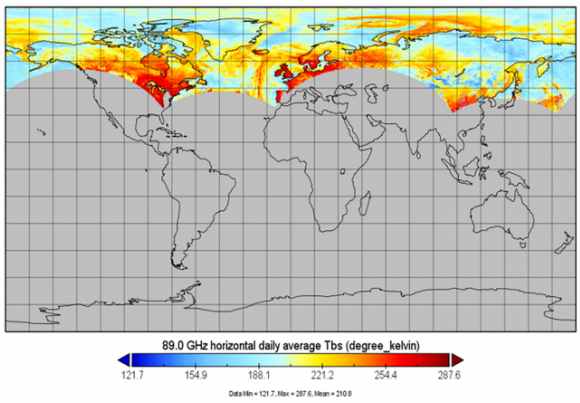

Figure 3. Data source visualization.

Open and view the HDF file through the EXE of HDF Explorer. Visualize the HDF data of ARMS-E through the viewer, and get Fig. 3. Through the visualization data and network query data, we can understand the location of the data we will process, the distribution of land and the general range of sea ice. It is convenient for us to classify the sea ice in the future, and we can also understand the general distribution of light temperature values in the Arctic region from the Fig. 3.

3 Methods

In microwave remote sensing, it can be divided into two categories: active microwave remote sensing and passive microwave remote sensing. But they all have one thing in common: they are not affected by atmosphere or clouds. So it plays a very important role in the survey of the polar region. Active microwave remote sensing is to obtain the information of sea ice type by means of the back scattering of microwave beam which is transmitted by satellite actively. Passive microwave remote sensing is through receiving the ground object's own radiation information, and then analysis of sea ice types [6].

Passive microwave sensor is also called radiometer. Radiometer is mainly used to measure the radiation signal of surface objects themselves. However, the spatial resolution of radiometer is relatively low, but it is very suitable for the analysis of sea ice type. Today, the SSM/I series of microwave radiometers on the U.S. defense weather satellite DMSP, and the AMSR-2 and AMSR-E sensors on the Japanese GPM-W and Aqua satellites, respectively, make it easy to identify sea ice types. The brightness temperature T_b we will use depends on the emissivity of the radiation layer of the object itself and the physical temperature T_{bin}. The formula is as follows:

$$T_b = f(T_{bin}, \epsilon) \tag{1}$$

And of course, the composition of various objects

and their properties and things like that affect their emissivity, and in sea ice things like their water content and their salinity and things like that affect temperature changes, and those changes are reflected in the brightness temperature. The difference between sea water and sea ice is even greater, so the radiometer can easily tell the difference between sea ice and sea water. The differences in microwave segments and polarization patterns of sea ice at different growth stages are also very large. Moreover, these differences can be directly reflected by the brightness temperature value, so in this paper, we can use microwave radiometer to identify the types of sea ice.

In the past studies, we can get some useful information. In the 89GHz frequency band, the polarization difference of one-year ice and multi-year ice is relatively small, while the polarization difference of seawater is relatively obvious in this frequency band. In order to show this difference, we compared light and temperature maps with data in the 19GHz, 37GHz and 89GHz bands [7]. Here we choose three typical areas we know from the Internet for comparison. Perennial ice is north of Greenland (84°–85.5°N, 31.5°–36°W). The annual ice is in the Kara Sea (76.5°–78° N, 77°–79°E). Open water (73°–75°N,35°–36.5°E). The brightness temperature values of AMSRE data in these three regions are read, and then the average values of the whole region and the whole month are calculated to get the graph of the variation of brightness temperature of these three types of sea surface with the observed frequency band in this month. Fig. 1. shows the results calculated in January 2017. We can see from this result that the polarization difference between multi-year ice and one-year ice at 89GH is very small. The polarization difference in open water is quite large. Fig. 4. emissivity diagrams of seawater, one-year ice, and multi-year ice at an incident Angle of 50°.

It can also be seen from Fig. 4. that the brightness temperature of multi-year ice at 89GHz is lower than that of one-year ice except for the difference in polarization [8]. The emissivity of horizontal polarization and vertical polarization of ice rarely fluctuates greatly due to the influence of frequency [9]. As for the double-polarization emissivity of sea water and multi-year ice, with the increase of frequency, the sea water shows an increase, while the multi-year ice is on the contrary, continuously decreasing. For the emissivity of the same ground object under different polarization modes, it can be seen that for all frequencies within 100GHz, no matter

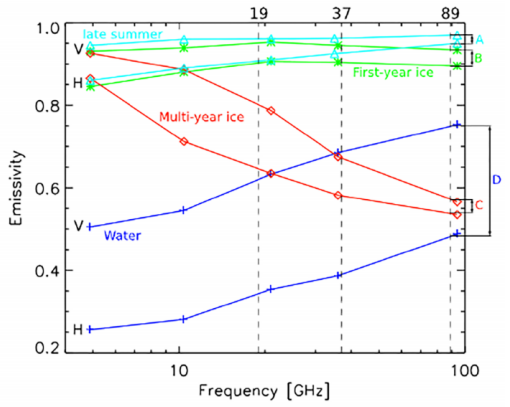

Figure 4. Variation of brightness temperature with observed frequency band (WATER: Water surface; The ice has been frozen for many years. It was First year ice. H: horizontal polarization; V: vertical polarization).

seawater, one year ice or multi-year ice, their emissivity under vertical polarization is greater than that under horizontal polarization [10]. Usually this happens when the emission comes mainly from the surface of the object, because the Fresnel reflection coefficient of the horizontally polarized object is greater than that of the vertically polarized object [11]. At the same time, it can be found that the emissivity difference between vertical polarization and horizontal polarization of seawater is the largest, and that of one-year ice is the smallest, while the emissivity difference of multi-year ice increases first and then decreases with the increase of frequency. Therefore, combining the polarization difference with the radiant brightness temperature can It is good to distinguish between sea water, one year ice and many years ice [12].

Based on the above classification principle, this paper first selects and corrects the problem data, and then uses MATLAB to achieve sea ice classification based on Otsu algorithm.

3.1 Data filtering method

In the low frequency band, the influence of cloud and water vapor on 36GHz data is relatively small, while the influence on 89GHz data is relatively large. In cloudless weather conditions, the polarization ratio of 89GHz data and 36GHz data is stable. When there are external factors such as cloud and water vapor, the polarization ratio will be affected Therefore, in this paper, the affected 89GHz data were screened by polarization ratio to eliminate the interference of cloud and fog in sunny days.

We can first select 36GHz data and 89GHz data in sunny days in 2017 as sample point data. Then, the

polarization ratio was calculated respectively to draw the scatter plots of the polarization ratio of the selected 89GHz and 36GHz sample data, as shown in the Fig. 5. The formula for calculating the polarization ratio is shown in Equation (2):

$$\mathrm{PR} = \frac{\mathrm{TB_V} - \mathrm{TB_H}}{\mathrm{TB_V} + \mathrm{TB_H}} \tag{2}$$

Where, PR represents polarization ratio. TB represents the vertical polarization brightness temperature of microwave data. TB represents the brightness temperature of microwave horizontal polarization of data.

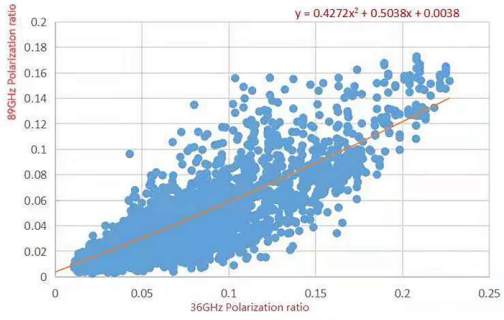

Figure 5. PR_{89} and PR_{36} scatter plots.

The solid curve is considered to be the boundary where the data is affected, and the data points below the curve need to be corrected. The scatter diagram shows the relationship between PR_{89} and PR_{36}. On the basis of the scatter diagram, the abscissa PR_{36} is divided into several intervals, and the mean value and standard deviation of the ordinate PR_{89} in each interval are calculated. The least square optimal fitting curve is drawn with the mean value minus standard deviation twice in each interval, and the curve is approximate to the quadratic equation. It can be expressed by the following Equation (3):

$$\mathrm{PR}_{89} = a(\mathrm{PR}_{36})^2 + b\mathrm{PR}_{36} + c \tag{3}$$

Where, PR_{89} represents the polarization ratio of 89GHz data. PR_{36} represents the polarization ratio of 36GHz data. Type(3): a=0.4272, b=0.5038, c=0.0038. Apply this relationship curve to the 89GHz data to screen out the affected 89GHz data. As shown in Fig. 6.

3.2 Data correction method

Since 36GHz data is relatively stable and weakly affected by cloud and water vapor, 36GHz data can be used to correct the influence of cloud and water vapor on 89GHz data By selecting a large number

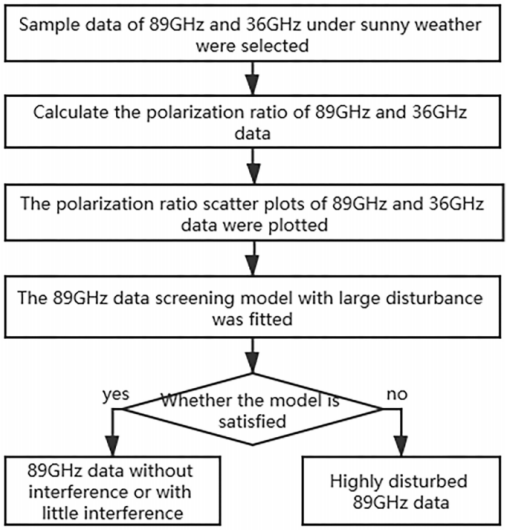

Figure 6. Data filtering flow chart.

of sample points of PR89 data and PR36 data under cloudless weather conditions, and then using the sample points to carry out fitting calculation, we find out a relationship expression representing 89GHz data and 36GHz data. Through many experiments, it is found that unary model can achieve better fitting effect. The modified model fitted out is shown in Equation (4):

$$P' = a_1P^3 + b_1P^2 + c_1P + d_1 \tag{4}$$

Where, P' is the PR data after resampling, and is the PR. data after correction. The parameter in Equation (4): $a_1 = 30.876, b_1 = 10.5726, c_1 = 1.5483$, Equation (4) is used to correct the screened 89GHz data affected by the external environment such as cloud and water vapor.

3.3 Classification methods of sea ice

We will use the Classification Learner APP in MATLAB to classify the sea ice we extracted. Through Fig. 4. the bright temperature changes with the observed frequency band, and the proposed classification principle, the polarization difference and radiation bright temperature values are combined to distinguish seawater by using the fine tree theory of MATLAB decision tree one year ice and many years ice decision tree is a basic classification method in machine learning. Decision tree is also equivalent to a regression algorithm. Decision tree is a tree built based on strategic choices. The idea of decision tree is mainly derived from Otsu algorithm.

3.3.1 Otsu algorithm

Otsu algorithm selects a threshold based on the variance between the image data. The principles are

as follows:

It is assumed that the threshold can divide the images of L level data into two categories:

The corresponding probability of $C_0 \in [0, T]$ and $C_1 \in [T+1, L+1]$ is:

$$p_i = \frac{n_i}{N} \tag{5}$$

Where, N is the total number of pixels, n_i is the number of pixels with the data level i, and there is $p_i \geq 0, \sum_{i=0}^{L-1} p_i = 1$. The probability of C_0 and C_1 is:

$$w_0 = p_r(C_0) = \sum_{i=0}^{T} p_i = w(T) \tag{6}$$

$$w_1 = p_r(C_1) = \sum_{T+1}^{L+1} p_i = 1 - w(T) \tag{7}$$

The mean values of C_0 and C_1 are as follows:

$$u_0 = \sum_{i=0}^{T} \frac{ip_i}{w_0} = \frac{u(T)}{w(T)} \tag{8}$$

$$u_1 = \sum_{i=T}^{L-1} \frac{ip_i}{w_1} = \frac{\bar{u} - u(T)}{1 - w(T)} \tag{9}$$

Where, $\bar{u} = \sum_{i=0}^{L-1} ip_i$ is the mean of the image. The inter-class variance of C_0 and C_1 is:

$$\sigma_g^2 = w_0 w_1 (u_1 - u_0)^2 \tag{10}$$

The optimal classification threshold T^* of sea ice and seawater should make the largest inter-class variance, that is:

$$T^* = \arg \max_{0 \leq T \leq L-1} \sigma_g^2 \tag{11}$$

3.3.2 Sea ice distribution detection based on Otsu algorithm

The Otsu algorithm is used to deal with 89GHz polarization difference P, and the classification threshold of sea ice and seawater is obtained, and then the distribution information of Arctic sea ice is obtained. Fig. 7. is the flow chart of the sea ice distribution detection method. The basic steps are as follows:

(1) Data preprocessing

Radiometric calibration, masking, and abnormal data processing (When there is too much difference between a data and the median of the data in its central window, the data is defined as an abnormal data, instead of the median value of the data in the window).

(2) Calculate polarization difference

The polarization difference P=89V-89H is calculated by using the vertical and horizontal polarization of 89GHz.

(3) Determining the optimal classification threshold for sea ice and seawater

Select sample points and process polarization difference P based on Otsu algorithm, and obtain the optimal classification threshold T of sea ice and seawater.

(4) Obtain Sea ice distribution map

The polarization difference P is classified according to the threshold T, and the Arctic sea ice distribution map is obtained.

(5) Result verification

The results are compared with the results obtained from NSIDC(National Snow and Ice Data Center) and NASA-Team algorithm.

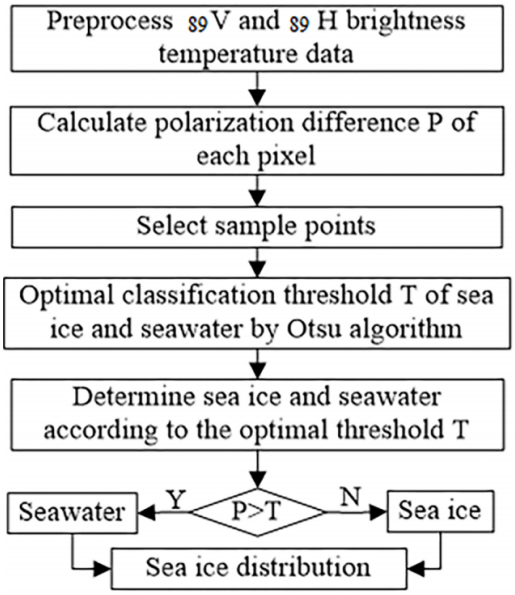

Figure 7. Flow chart of sea ice distribution for 89GHz data.

4 Results and Validation

In this paper, the distribution of sample points calculated by the fine tree theory of MATLAB decision tree is used to draw the classification results of our classification result chart, as shown in Fig. 8. Inside, 1 is multi-year ice, 0 is land, 2 is open water, and 3 is one-year ice.

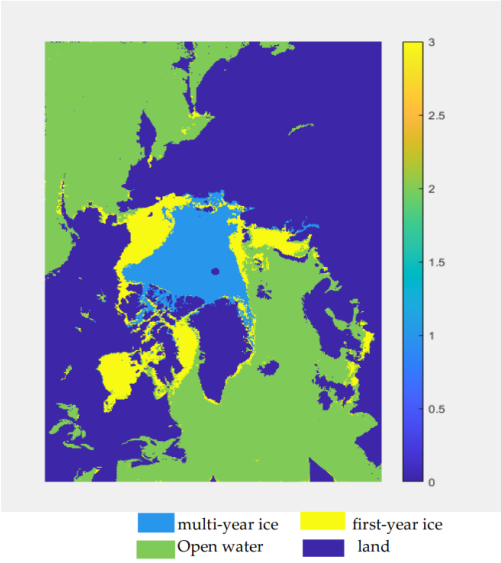

Figure 8

The principle of classification in this paper starts from the same starting point as the principle of other papers and is arranged relative to each other by using their polarization values in characteristic bands. However, the classification method used in this paper was not ENVI, but MATLAB decision tree. Therefore, in the verification of the results, we found the classification result in January 2017 by combining radiometer and scatter remote with threshold segmentation method used by Wang Yi as shown in Fig. 1.

From Fig. 1 can see roughly can come to a conclusion, and we try to this article classification result is largely the same, so the method is feasible, this article use but because of the use of the software and the way is different, will make a big difference on the data calculation, Fig. 1 has certain difference in the output results.

5 Conclusion

In this paper, the sea ice types in the Arctic are analyzed based on the data of 89GHz frequency band of AMSR-E microwave remote sensing radiometer. The spatial resolution of 89GHz frequency band is almost twice that of other low frequency bands. The data is relatively stable, but it is greatly affected by clouds and water vapor in this frequency band. There are a lot of mature algorithms to invert the types of sea ice in the low frequency band. Therefore, it is of great significance to use high-frequency data for research in this paper. This paper is a classification of Arctic sea ice by ENVI combined with the fine tree theory in Matlab decision tree.

This method may have some errors in data calculation. Decision tree generation algorithm is to generate the decision tree recursively, cannot be terminated, so the decision tree classification precision, often to the training data set classification accuracy, but the unknown data sets are not so accurate, there is a serious fitting issue, the complexity of the data can affect the accuracy of the results, but this is also a kind of new attempt, the advantages and disadvantages of this method need to be studied.

Conflicts of Interest

The authors declare that they have no conflicts of interest.

Acknowledgement

This work was supported without any funding.

References

[1] Cavalieri, D. J. (1994). A microwave technique for mapping thin sea ice. *Journal of Geophysical Research: Oceans*, 99(C6), 12561-12572. [CrossRef]

[2] Cavalieri, D. J., Gloersen, P., & Campbell, W. J. (1984). Determination of sea ice parameters with the Nimbus 7 SMMR. *Journal of Geophysical Research: Atmospheres*, 89(D4), 5355-5369. [CrossRef]

[3] Cavalieri, D. J., & Parkinson, C. L. (2012). Arctic sea ice variability and trends, 1979–2010. *The Cryosphere*, 6(4), 881-889. [CrossRef]

[4] Comiso, J. C., & Nishio, F. (2008). Trends in the sea ice cover using enhanced and compatible AMSR-E, SSM/I, and SMMR data. *Journal of Geophysical Research: Oceans*, 113(C2).[CrossRef]

[5] Comiso, J. C. (1986). Characteristics of Arctic winter sea ice from satellite multispectral microwave observations. *Journal of Geophysical Research: Oceans*, 91(C1), 975-994. [CrossRef]

[6] Ulaby, F. T., Kouyate, F., Brisco, B., & Williams, T. L. (1986). Textural information in SAR images. *IEEE Transactions on Geoscience and Remote Sensing*, (2), 235-245. [CrossRef]

[7] Soh, L. K., Tsatsoulis, C., Gineris, D., & Bertoia, C. (2004). ARKTOS: An intelligent system for SAR sea ice image classification. *IEEE Transactions on geoscience and remote sensing*, 42(1), 229-248. [CrossRef]

[8] Ressel, R., Frost, A., & Lehner, S. (2015). A neural network-based classification for sea ice types on X-band SAR images. *IEEE Journal of Selected Topics in Applied Earth Observations and Remote Sensing*, 8(7), 3672-3680. [CrossRef]

[9] Cavalieri, D. J., Parkinson, C. L., Gloersen, P., Comiso, J. C., & Zwally, H. J. (1999). Deriving long-term time series of sea ice cover from satellite passive-microwave

multisensor data sets. *Journal of Geophysical Research: Oceans*, 104(C7), 15803-15814. [CrossRef]

[10] Nghiem, S. V., Steffen, K., Kwok, R., & Tsai, W. Y. (2001). Detection of snowmelt regions on the Greenland ice sheet using diurnal backscatter change. *Journal of Glaciology*, 47(159), 539-547. [CrossRef]

[11] Gough, S. R. (1972). A low temperature dielectric cell and the permittivity of hexagonal ice to 2 K. *Canadian Journal of Chemistry*, 50(18), 3046-3051. [CrossRef]

[12] Li, Y., & Cao, J. (2023). Adaptive Binary Particle Swarm Optimization for WSN Node Optimal Deployment Algorithm. *IECE Transactions on Internet of Things*, 1(1), 1-8. [CrossRef]

[13] Fang, F. A. N. G., Tan, W., & Liu, J. Z. (2005). Tuning of coordinated controllers for boiler-turbine units. *Acta Automatica Sinica*, 31(2), 291-296.

[14] Wang, N., Fang, F., & Feng, M. (2014, May). Multi-objective optimal analysis of comfort and energy management for intelligent buildings. In *The 26th Chinese control and decision conference (2014 CCDC)* (pp. 2783-2788). IEEE.

[15] Fang, F., Jizhen, L., & Wen, T. (2004). Nonlinear internal model control for the boiler-turbine coordinate systems of power unit. *PROCEEDINGS-CHINESE SOCIETY OF ELECTRICAL ENGINEERING*, 24(4), 195-199.

Yue Zhao Currently majoring in electronic Information in College of Information Science and Engineering, Henan University of Technology. The research direction is remote sensing in sea ice concentration.

Xingdong Wang Currently working at the School of Information Science and Engineering, Henan University of Technology. His current research interests include remote sensing, GIS(geographic information system).

Changfeng Luo From 2017 to 2021, he graduated from the computer department of Henan University of technology with a bachelor's degree. His current research interests is Spatial information and digital technology.